# Black carbon sources constrained by observations in the Russian high Arctic



| | |
|---|---|
| Journal: | *Environmental Science & Technology* |
| Manuscript ID | es-2016-058322.R1 |
| Manuscript Type: | Article |
| Date Submitted by the Author: | n/a |





| | |
|---|---|
| Complete List of Authors: | Popovicheva, Olga; Moscow State University, Institute Nuclear Physics<br>Evangeliou, Nikolaos; Norwegian Institute for Air Research (NILU), Department of Atmospheric and Climate Research<br>Eleftheriadis, Konstantinos; N.C.S.R. , Institute of Nuclear Techn. & radiation Protection<br>Kalogridis, Athina Cerise; N.C.S.R. , Institute of Nuclear Techn. & radiation Protection<br>Movchan, Vadim; Arctic Antarctic Research Institute, St. Petersburg, Russia<br>Sitnikov, Nikolay; Central Aerological Observatory (CAO)<br>Eckhardt, Sabine; NILU,<br>Makshtas, Alexander; Arctic Antarctic Research Institute, St. Petersburg, Russia<br>Stohl, Andreas; Norwegian Institute for Air Research (NILU), Department of Atmospheric and Climate Research |
| | |

# Black carbon sources constrained by observations in the Russian high Arctic

Olga B. Popovicheva[1], Nikolaos Evangeliou[2,*], Konstantinos Eleftheriadis[3], Athina C. Kalogridis[3], Vadim Movchan[4], Nikolay Sitnikov[5], Sabine Eckhardt[2], Alexander Makshtas[4], Andreas Stohl[2]

[1] Scobeltsyn Institute of Nuclear Physics, Lomonosov Moscow State University (MSU), Moscow, Russia.

[2] NILU - Norwegian Institute for Air Research, Department of Atmospheric and Climate Research (ATMOS), Kjeller, Norway.

[3] N.C.S.R. "Demokritos", Institute of Nuclear and Radiological Sciences & Technology, Energy & Safety, 15341, Ag. Paraskevi, Attiki, Greece.

[4] Arctic Antarctic Research Institute, St. Petersburg, Russia.

[5] Central Aerological Observatory (CAO), Moscow Region, Russia.

*Corresponding author: N. Evangeliou, NILU - Norwegian Institute for Air Research, Department of Atmospheric and Climate Research (ATMOS), Kjeller, Norway.

Tel: +47 63 89 81 89, Fax: +47 63 89 80 50, E-mail: Nikolaos.Evangeliou@nilu.no

**WORD COUNT**

Abstract + Manuscript + Acknowledgement + SI = 4700

Figures 1 (300) + Figure 2 (600) + Figure 3 (300) + Figure 4 (600) + Figure 5 (300) = 2100

**TOTAL = 6800 < 7000**

**ABSTRACT:** Understanding the role of short-lived climate forcers like black carbon (BC) at high northern latitudes in climate change is hampered by the scarcity of surface observations in the Russian Arctic. In this study, highly time resolved Equivalent BC (EBC) measurements during a ship campaign in the White, Barents and Kara Seas in October 2015 are presented. The measured EBC concentrations are compared with BC concentrations simulated with a Lagrangian particle dispersion model coupled with a recently completed global emission inventory to quantify the origin of the Arctic BC. EBC showed increased values (100–400 ng $m^{-3}$) in the Kara Strait, Kara Sea, and Kola Peninsula, and an extremely high concentration (1000 ng $m^{-3}$) in the White Sea. Assessment of BC origin throughout the expedition showed that gas flaring emissions from the Yamal/Khanty-Mansiysk and Nenets/Komi regions contributed the most when the ship was close to the Kara Strait, north of 70˚N. Near Arkhangelsk (White Sea), biomass burning in mid–latitudes, surface transportation, and residential and commercial combustion from Central and Eastern Europe were found to be important BC sources. The model reproduced observed EBC concentrations efficiently, building credibility in the emission inventory for BC emissions at high northern latitudes.

## 1. INTRODUCTION

Short-lived climate forcers are aerosols and gases that cause radiative forcing [1,2] and have lifetimes of less than a few years [3,4]. Light-absorbing aerosols are of particular interest, since they have a warming effect that is strongest over highly reflective surfaces (e.g., clouds, snow and ice) [5]. Furthermore, their deposition on snow and ice decreases surface albedo, which can enhance melting [6,7] and trigger surface warming. Most of the radiation absorption of accumulation-mode aerosol is due to black carbon (BC) [8]. BC also influences cloud radiative properties [9,10]. BC originates from incomplete combustion, e.g., of biomass or fossil fuels [1,11]. Freshly emitted BC is hydrophobic but ageing in the atmosphere changes its properties to a more hydrophilic state [12]. It is an important constituent in Arctic Haze, a phenomenon that is primarily the result of long-range pollution transport from sources outside the Arctic [5,7,13,14]. The majority of the Arctic BC originates from anthropogenic sources, especially industrial applications, residential combustion, and diesel transportation activities [15], while other important sources include fires in boreal forests and agricultural regions especially from spring to fall [16–18].

Near the surface, about 50% of the BC north of 60°N originates from Russia [19], where emission inventory data are highly uncertain [20]. Emissions from flaring of gas associated with oil production are prone to particularly high uncertainty because both activity data and emission factors are largely lacking. According to the Global Gas Flaring Reduction Partnership (GGFR) (http://www.worldbank.org/en/programs/gasflaringreduction), nearly 50 billion $m^3$ of gas are flared in Russia annually. The Russian flaring emissions in the Yamal and Khanty-Mansiysk regions are directly within the major low-altitude pathway of sub-Arctic air masses penetrating into the Arctic [16] and thus Stohl et al. [21] estimated that they contribute about 42% of the annual average BC surface concentrations in the Arctic..

However, limited measurements are available that would enable constraining this particular source of BC in the Russian Arctic. For instance, in the whole Russian territory north of 50°N, continuous measurements of equivalent BC (EBC) are performed only at Tiksi station (71.36°N; 128.53°E) [22,23], which is far from the major industrial sources in Russia. Based on isotope measurements, one recent observational study [24] suggests that the contribution of gas flaring emissions to BC at Tiksi is lower than estimated by Stohl et al. [21]. However, new bottom-up inventories [25,26] contain gas flaring emissions that are even higher than those used by Stohl et al. [19]. To clarify the role of gas flaring emissions, any EBC

measurements from regions closer to the oil production facilities of Russia would be extremely valuable, In these regions, BC has been measured only with low time resolution during a few ship campaigns [21,27–29]. However, to relate such measurements to particular source regions, measurements with high time resolution are necessary. In a comparison with the few available observations, modeled BC concentrations were found to be too low [21], but a comprehensive analysis was not possible because of the low time resolution of these measurements.

In the present study, we report highly time resolved EBC concentrations measured during the "Sever-2015" expedition through the White Sea, Barents Sea, and Kara Sea in October 2015. We compare the EBC measurements recorded during the cruise with predicted BC concentrations simulated with a Lagrangian particle dispersion model (LPDM). Furthermore, we investigate and quantify the origin of the BC observed during the cruise using modeling results coupled with the most recent emission inventory for BC. This is done to assess how the oil and gas industrial emissions in high northern latitudes affect Arctic BC.

## 2. METHODOLOGY

**2.1 Expedition and Analysis of Equivalent Black Carbon.** The expedition "Sever-2015" was carried out onboard the research vessel "Akademik Treshnikov" of the Russian Arctic and Antarctic Research Institute from 9 to 25 October 2015. The ship is the modern vessel of RMRS (Russian Maritime Register of Shipping, class notation KM Arc7AUT2) and it uses three propulsion WÄRTSILÄ diesel 4-stroke engines with 600 rpm. The ship track in the Arctic Ocean and the research vessel are shown in Figure S 1 together with the main gas flaring facilies. The cruise started on 10 October from the port of Arkhangelsk (64.58°N, 40.50°E; point A on the map), and continued through the delta of the Dvina river towards the White Sea and Kanin Nos (point 1 in Figure S 1) in the Barents Sea. Then it passed the Kara Strait (point 2 in Figure S 1) and the Kara Sea until it reached the archipelago Severnaya Zemlya (79.35°N, 101.83°E; point B). After a stay of two days near the research station "Ice Base Cape Baranova" on the Bolshevik Island (from 15 to 17 October 2015), the ship turned back. A storm forced the ship to moor in the Kara Sea (point 3 in Figure S 1) from 19 to 21 October before it could continue its return journey to Arkhangelsk, where it arrived on 25 October. Meteorological data (temperature, apparent wind speed and direction) during the cruise were obtained from the Vaisala maritime observation system MAWS-420. Real wind

direction and speed was estimated from the aforementioned data. Surface air temperature, pressure, and wind data are shown in Figure S 2, respectively.

Aerosol EBC concentrations were determined continuously using an aethalometer purposely designed by the Moscow State University (MSU) and Central Aerological Observatory (CAO) for ship campaigns. In this instrument, light attenuation caused by the particles depositing on a quartz fiber filter is measured at three wavelengths (450, 550, and 650 nm). The light attenuation coefficient of the collected aerosol was calculated with the method of Hansen and Rosen [30]. EBC concentrations were determined continuously by converting the time-resolved light attenuation to the EBC mass corresponding to the same attenuation and characterized by a specific mean mass attenuation coefficient. This calibration parameter was derived during parallel long-term measurements against an AE33 aethalometer (Magee Scientific) that operates at the same three wavelengths (450, 550, and 650 nm).

Attenuation coefficient b$atn$ is defined as:

$$batn = A(m^2) \cdot \delta ATN/V(m^3) \qquad (1)$$

where $A$ is the filter exposed area, and $V$ is the volume of air sampled and $\delta ATN$ is the light attenuation defined as follows:

$$\delta ATN = \ln(I_o/I) \qquad (2)$$

where $I_o$ and $I$ is the light intensity transmitted through unexposed and exposed parts of the filter, respectively. Good linear correlation between the aethalometer's attenuation coefficient $batn$ and the EBC concentrations calculated with the AE33 aethalometer (at 660 nm) was achieved ($R^2 = 0.92$, see Figure S 3). This allowed estimation of EBC mass concentrations using the regression slope and intercept between $b_{atn}$ at 650 nm and EBC of the AE33 aethalometer at 660 nm:

$$EBC(ng\ m^{-3}) = 3.3 \times 10^5 \cdot A(m^2) \cdot \delta ATN/V(m^3) \qquad (3)$$

where $3.3 \times 10^5$ is the correction factor that includes the specific mass absorption coefficient for the MSU aethalometer calibrated against the AE33 aethalometer assuming the Mass Absorption Cross-section (MAC) adopted by AE33 equal to 9.89 $m^2\ g^{-1}$ [31]. The uncertainty of EBC measurements from both aethalometers depends on the accuracy of the MAC value used for the conversion of the light absorption coefficient to mass concentration. The constant MAC value adopted here is an approximation, assuming a uniform state of mixing for BC in

136 atmospheric aerosol. This can be considered a valid assumption in the case of background
137 aerosol measurements performed in this study. Absolute uncertainties of the reported MAC
138 values remain as high as 30–70% due to the lack of appropriate reference methods and
139 calibration materials [32].

140 The level of uncertainty (1-sigma) of EBC measurements was 30 ng $m^{-3}$ for six minutes
141 integration time. Aethalometer filters were changed manually at the latest when ATN values
142 approached 70 but at most times filters were changed at lower values. During rough and wet
143 weather conditions, water droplets or sea spray affected the measurements adding higher
144 noise to the recorded ATN signal. These short data periods were either excluded from the
145 dataset or, where possible, treated manually by establishing an adjusted baseline for the
146 reference ATN values.

147 To identify the cleanest location on the vessel (i.e., the spot least influenced by the ship
148 exhaust), particulate mass (PM) concentration was measured on all decks of the vessel using a
149 TSI DustTrak 8530 monitor. The best site for ambient aerosol monitoring was identified to be
150 at the foredeck, where the aethalometer was placed, while the spot most affected by the
151 exhaust pipe was found at about 10 m on the upper bridge (Figure S 1). A second
152 aethalometer of exactly the same type was therefore installed at this location to record
153 potential impact from ship pollution. EBC concentrations from the two aethalometers were
154 compared and the absence of contamination on the foredeck, where the aethalometer was
155 placed (clean air site), was assured. When the apparent wind was blowing from the back of
156 the vessel towards the clean air site on the foredeck, all aethalometer data were removed from
157 further analysis. For instance, such contamination might have occurred when the ship moored
158 near point 3 (Figure S 1) during the storm event and therefore these measurements were
159 removed from the dataset.

160 **2.2 Emissions and Modeling of Black Carbon.** The concentrations of BC were
161 simulated with version 10 of the LPDM FLEXPART (FLEXible PARTicle dispersion model)
162 [33,34]. The model was driven with operational meteorological analyses every three hours from
163 the European Centre for Medium-Range Weather Forecasts (ECMWF). The ECMWF data
164 had 137 vertical levels and a horizontal resolution of 1°×1°. Computational particles released
165 from the measurement locations were tracked back in time in FLEXPART's "retroplume"
166 mode [35]. Simulations extended over 30 d back in time, sufficient to include most aerosol
167 emissions arriving at the station, given a typical BC lifetime (□1 week). This enabled

identifying where the measured BC came from and allowed quantification of BC source contributions. The source contributions can also be displayed as a function of the time elapsed since the emission has occurred (i.e., ”age”), which can be shown as “age spectrum” consisting of stacked bars, where a bar’s color indicates the contribution of a certain age bin (0-1 days, 1-2 days,..., 29-30 days) (see **Figure 1**b). FLEXPART simulations were performed every hour during the cruise, with particles released from small boxes covering the latitude and longitude ranges of the ship track during the hour. The FLEXPART retroplumes consist of an emission sensitivity (often also called source-receptor relationship), which yields a simulated concentration in the receptor box when multiplied with gridded emissions from an inventory.

Emission fluxes were taken from the ECLIPSE (Evaluating the CLimate and Air Quality ImPacts of ShortlivEd Pollutants) version 5 emission dataset [36], which is available from the website of the International Institute for Applied Systems Analysis (IIASA) (http://www.iiasa.ac.at/web/home/research/researchPrograms/air/Global_emissions.html). This inventory is appropriate for use in our study, as it accounts for BC emissions from gas flaring from the main emitting facilities located west of Yamal Peninsula (Komi and Nenets distinct) and in Khanty-Mansiysk (south of Yamal Peninsula) [21]. Biomass burning (BB) sources, namely forest, peat, savanna, woodland fires, and from deforestation were adopted from the Global Fire Emissions Database, Version 3 (GFEDv3.1) [37]. As regards to anthropogenic sources, it includes industrial combustion and processes sector (IND) emissions from combustion happening in industrial boilers as well as emissions from industrial production processes. Residential and commercial sector (DOM) includes emissions from combustion in heating and cooking stoves and boilers in households and public and commercial buildings like malls, hospitals and schools. Waste treatment and disposal sector (WST) includes emissions from waste incineration and the treatment process. Transport sector (TRA) includes emissions from all land based transport of goods, animals and persons on road networks as well as off-road activities e.g. on railroads, agricultural and forest lands, construction sites. Shipping in in-land waters and domestic aviation are also included in this sector, but international shipping and aviation are treated as separate sectors. Finally, energy production and distribution sector (ENE) includes emissions from combustion processes in power plants and generators, emission related to distribution of energy to consumers, as well as emissions from gas flaring in oil facilities.

For our simulations, we assumed that BC has a density of 2000 kg $m^{-3}$ and follows a logarithmic size distribution with an aerodynamic mean diameter of 0.25 μm and a logarithmic standard deviation of 0.3. Each computational particle released in FLEXPART represents an aerosol population with a lognormal size distribution (see Stohl et al., 2005). This treatment of aerosol size distribution allows simulating several different types of particles, each with its own size distribution. Removal processes acting differently for the different particle sizes will then affect specific particle sizes. Assumed aerodynamic mean diameter and logarithmic standard deviation are used by FLEXPART's dry deposition scheme, which is based on the resistance analogy [38], and they are consistent with those used in other transport models [18,39]. Below-cloud scavenging was determined based on the precipitation rate taken from ECMWF. The in-cloud scavenging was based on cloud liquid water and ice content, precipitation rate and cloud depth from ECMWF [40]. The FLEXPART user manual (available from http://www.flexpart.eu) provides more information on FLEXPART's removal parameterizations. All FLEXPART results for the cruise can be viewed interactively at the URL http://niflheim.nilu.no/NikolaosPY/RusArctExp_2015.py.

## 3. RESULTS AND DISCUSSION

**3.1 Onboard EBC Measurements.** The EBC concentrations measured during the cruise are shown in **Figure 1**a. At the beginning of the expedition (10 October 2015) when the ship was in or near the port of Arkhangelsk (White Sea), high values of EBC were measured (hourly values up to 700 ng $m^{-3}$) probably due to local pollution. Only after the ship passed the industrial area of the Dvina river delta (10 October 2015 at 20:30), EBC dropped to below 100 ng $m^{-3}$. In the open White Sea, EBC was 40 ng $m^{-3}$, on average, but a small peak (~163 ng $m^{-3}$) was observed near the Kola Peninsula in the morning of 11 October (06:30). In the basin of the Barents Sea absorption was below the detection limit of the aethalometer, and only in the Pechora Sea (West of Kara Strait) on 12 October (06:30) EBC concentrations rose above the minimum detection levels again, gradually increasing up to 153 ng $m^{-3}$. In the Kara Strait EBC was strongly enhanced (~220 ng $m^{-3}$); concentrations kept increasing in the Kara Sea up to a maximum of 360 ng $m^{-3}$ (**Figure 1**a), in an area north of strong gas flaring emissions (see Figure 1 of Stohl et al.[21]). Notice that at remote Arctic stations, measured EBC concentrations are much lower, typically only around 10 ng $m^{-3}$ at this time of the year [41], which can be considered the typical Arctic background [42]. Hence, EBC values observed in the Barents Sea were relatively close to the background concentrations observed in other parts of the Arctic, whereas in the Kara Sea EBC concentrations were strongly enhanced compared to

this level. It is worth to note that the measured EBC concentrations are comparable to those reported by Stohl et al.[21] of about 200-400 ng $m^{-3}$ during a ship cruise in the Kara Sea in September 2011.

In the morning of 13 October (07:30), when the ship was in the Eastern Kara Sea, EBC dropped to 100 ng $m^{-3}$, then varied between 50 and 220 ng $m^{-3}$ until midnight of 14 October, before decreasing towards minimum detectable limits until archipelago Severnaya Zemlya. On 15 October (02:50) the ship moored in the Shokalsky's passage near station "Ice Base Cape Baranova" on the Bolshevik Island (Figure S 1) until 18 October, when the voyage back to Arkhangelsk started.

On the way back to Arkhangelsk, in the morning of 18 October we observed EBC concentrations reaching around 60 ng $m^{-3}$ (Figure 1a). While these concentrations were lower than those observed on the way to the Bolshevik Island, they are still much higher than the Arctic background. From 19 October at 10:00 to 21 October at 22:00 the ship maneuvered in the central part of the Kara Sea searching for mooring stations. At that time BC varied to about 200 ng $m^{-3}$. However, due to frequent changes of the ship's course, the ship's exhaust might have been transported to the clean air site (see Figure S1) via complicated pathways. Therefore, enhanced EBC measurements during this period were excluded from further analysis. On 21 October, when the vessel continued its voyage to Arkhangelsk, relatively high EBC concentrations were measured, while on 22 October at 18:00 no absorption could be measured. On 23 October, the ship passed through the Kara Strait recording EBC concentrations of up to 250 ng $m^{-3}$. Measured EBC concentrations declined substantially in the Barents Sea, until the ship reached the Kola Peninsula where a small peak was recorded on 24 October at around 6:00. Then EBC rapidly increased along the Dvina River in the White Sea with a maximum of about 1100 ng $m^{-3}$ on 24 and 25 October 2015. When the ship arrived at the port of Arkhangelsk, EBC concentrations of 1500 ng $m^{-3}$ were measured. Although we initially considered these high EBC concentrations close to the port of Arkhangelsk as local pollution, in the next section we show that this was actually not the case.

### 3.2 Analysis of BC sources observed during the expedition.

Figure 1b shows the modeled concentrations color-coded according to their age since emission in contrast to the measurements, while in Figure 1c the modeled concentrations are separated according to the different emission categories. It was already mentioned that the

ECLIPSE inventory includes anthropogenic and biomass burning emission sources adopted from GFEDv3.1 [36,37]. Flaring emissions dominate the emissions from the energy (ENE), sector south of the Barents and Kara Seas. Generally, the model captured periods with enhanced concentrations (e.g., in the Kara Sea during both the outward and return trip) and such with very low concentrations (e.g., in the Barents Sea) quite well. One exception is the first few hours of the cruise, when FLEXPART retroplumes showed that clean air masses from the Arctic reached the vessel in the port of Arkhangelsk. It is, however, very likely that the high measured EBC concentrations were caused exclusively by local pollution within the port, which cannot be captured by FLEXPART.

In the morning of 12 October, FLEXPART strongly overestimated the measured BC concentrations (shortly before the ship passed through the Kara Strait), then underestimated them by about 50%, and finally captured them almost exactly in the Kara Sea (13 October). As shown in Figure 1c, the modeled concentrations during this period had a large flaring contribution (ENE in Figure 1c). The measurements during this period thus enable us constraining the rather uncertain gas flaring emissions. Before the highest modeled BC peak on 12 October, retroplumes arrived straight from the east, with very little influence from the continent. At the time of the model peak, however, the retroplume encountered the northern parts of a strong cyclone centered over the Urals during the previous days. As a consequence, the retroplume turned direction over the Nenets and Komi regions and almost exactly where the ECLIPSE inventory places very high gas flaring emissions, resulting in very high values of the footprint emission sensitivity (Figure 2a) and source contributions (Figure 1c). This complex situation prevailed only for about 3 hours. After that, the retroplume circled the whole cyclone and this situation prevailed constantly for more than a day and during the entire passage of the Kara Sea (see Figure 2c and 3d). Based on the above analysis, it is likely that the modeled BC peak on 12 October is a result of the model not capturing the complex meteorological situation accurately enough. Even a small shift in the location of where the retroplume turned (Figure 2a) would have produced much smaller simulated BC concentrations. When the meteorological situation was more stable, the model captured the measured EBC concentrations rather well, especially on 13 October, when gas flaring emissions from the Yamal and Khanty-Mansiysk region contributed strongly. This suggests that gas flaring emissions for this region in the ECLIPSE inventory are in the right order of magnitude, perhaps with a slight tendency towards overestimation in the Nenets and Komi regions.

The very small EBC values in the Severnaya Zemlya archipelago were also well captured by FLEXPART (Figure 1b). During this time, the retroplumes showed transport from the Arctic Ocean, with very little influence from land sources. Figure 3a and b depict FLEXPART daily average emission sensitivities calculated when the vessel arrived to Severnaya Zemlya (14 October 2015) and when it departed (18 October 2015). Winds shifted on 18 October, with retroplumes arriving again first from southerly directions and thus increasing the potential for BC uptake over the land. Indeed, both measured and modeled BC concentrations increased again on 18 October.

On the way back, measured EBC concentrations in the Kara Sea were again captured quite accurately by FLEXPART. On 19 to 20 October, BC originated mainly from the Russian gas flaring sites of Yamal and Khanty-Mansiysk, confirming that these emissions appear to be well captured by the ECLIPSE inventory. From the afternoon on 20 October, air arrived straight from the west and was not influenced anymore by sources on the continent. This was also the case on 21 October when air came from the north. Measurements also showed decreasing EBC concentrations from 20 to 21 October (from 135 ng $m^{-3}$ on 20 October at 10:00 to near the detection limit on 21 October at 2:00).

On 22 October, as the ship approached the Kara Strait, air arrived from the southwest and gas flaring emissions from the Nenets and Komi regions were sampled again, similar to 12 October. This time, the model overestimated the measured EBC concentrations only slightly. Nevertheless, together with the results from the outward journey, this may suggest that flaring emissions in the Nenets and Komi regions are somewhat overestimated in the ECLIPSE inventory.

On 24 to 25 October, measured EBC values in the White Sea reached more than 1000 ng $m^{-3}$ and FLEXPART simulated similarly high BC values. The retroplumes at this time arrived from the southwest and brought polluted air masses mainly from Eastern Europe (Figure 4a). An example of the source contributions for 25 October at 00:00 is shown in Figure 4b and 5c. At that time, the modeled concentration of BC was 1310.5 ng $m^{-3}$, which is close to the observed values in the range from 696 to 1501 ng $m^{-3}$. About 10% (130.8 ng $m^{-3}$) originated from fires over Ukraine (Figure 4c), whereas about 90% originated from anthropogenic sources mainly in Central and Eastern Europe (Figure 4b). Excluding biomass burning, surface transportation contributed about 38%, residential and commercial

combustion sources up to 41%, gas flaring contributed about 8% and emissions from industrial combustion and processing between 1–2%.

Figure 5 depicts calculated normalized bias for the daily average measured EBC and modeled BC concentrations along the ship track in the White, Barents and Kara Seas. This statistic expresses the difference (model-observed) over the observed values. It is a useful indicator for assessing the models' performance because it avoids over-inflating the observed range of values, especially at low concentrations and it is used here to show the locations where modeled concentrations over- or underestimated the observations. The model is least biased when the gas flaring sources contribute the most to surface concentrations of BC, namely in the Pechora Sea (west of Kara Sea), in the Kara Strait and in the Kara Sea on the way to the Bolshevik Island, as well as in the middle of the Kara Sea (point 3 in Figure S 1), and close to the port of Arkhangelsk on the way back to Arkhangelsk. The extremely low concentrations calculated by the model in the beginning of the cruise in contrast to the high EBC concentrations (≈700 ng $m^{-3}$) led to negative biases near the port of Arkhangelsk and in the industrial area of Dvina river delta. On the contrary, the lack of absorption in the aethalometer near the Bolshevik Island from 15 to 17 October resulted in significant overestimated predicted BC concentrations by the model and high positive biases (Figure 5).

The very good agreement ($R^2 = 0.76$) between modeled and measured concentrations was confirmed by the root mean square error (RMSE). Whereas $R^2$ is a relative measure of fit, RMSE is an absolute measure of fit. It can be interpreted as the standard deviation of the unexplained variance; hence it is in the same units as the response variable. Lower values of RMSE indicate better fit. RMSE is a good measure of how accurately the model predicts the response, and is the most important criterion for fit if the main purpose of the model is prediction. The RMSE when including all data was estimated to be 230 ng $m^{-3}$. This high value is more or less expected here considering that the RMSE calculates the square error, hence it is very sensitive to larger errors. In the present case, if the points from the initial period of the cruise (Arkhangelsk and Dvina river industrial area) that were subject to local pollution are excluded, the RMSE falls to 85 ng $m^{-3}$, which is very low compared to the range of values observed during the cruise (0–1500 ng $m^{-3}$).

Overall, we found that the model had no systematic bias compared to the observations, which supports the validity of the ECLIPSE emission inventory for northern Russia. The good agreement especially in the region where flaring emissions are important suggests that flaring

emissions are also captured quite well in this inventory. This is particularly true for the Yamal and Khanty-Mansiysk regions, whereas there may be some overestimation of flaring emissions in the Nenets and Komi regions. Local pollution cannot be captured neither by our model due to poor temporal and spatial resolution of the available operational wind fields, nor by the emission inventory used (available in 0.5° resolution). When local pollution was insignificant (e.g., in regions far from urban and industrial areas), emissions from residential and commercial combustion, as well as surface transportation were also captured well.

## ASSOCIATED CONTENT

### Supporting Information

Figure S 1 shows the ship track of the research vessel "Akademik Treshnikov" in the Arctic Ocean and the main flaring facilities located in high latitudes. Figure S 2 depicts the measured meteorological conditions during cruise namely surface air temperature and pressure, and wind velocity and direction. Finally, Figure S 3 shows the quality of the EBC measurements (QA/QC) in terms of comparison of attenuation coefficients of the aethalometers used onboard (MSU) against EBC concentrations obtained with the AE33 aethalometer. This material is available free of charge via the Internet at http://pubs.acs.org.

## ACKNOWLEDGEMENTS

The present study was conducted in the framework of Roshydromet CNTP 1.5.3.4. The authors would like to thank the expedition leader V.T. Sokolov for his support. Financial support from RFBR-VAST 15-5554020 is kindly appreciated. We would also like to acknowledge the project entitled "Emissions of Short-Lived Climate Forcers near and in the Arctic (SLICFONIA)", which is funded by the NORRUSS research program of the Research Council of Norway (Project ID: 233642). Finally, we thank IIASA (especially Chris Heyes and Zig Klimont) for providing the BC emission dataset. The data used can be accessed upon request to the corresponding author of this manuscript.

## REFERENCES

(1) Bond, T. C.; Doherty, S. J.; Fahey, D. W.; Forster, P. M.; Berntsen, T.; Deangelo, B. J.; Flanner, M. G.; Ghan, S.; Kärcher, B.; Koch, D.; et al. Bounding the role of black carbon in the climate system: A scientific assessment. *J. Geophys. Res. Atmos.* **2013**, *118* (11), 5380–5552.

(2) IPCC. *Climate Change 2013: The Physical Science Basis. Contribution to the Fifth Assessment Report of the Intergovernmental Panel on Climate Change.*; Stocker, T. F., Qin, D., Plattner, G.-K., Tignor, M. M. B., Allen, S. K., Boschung, J., Nauels, A., Xia, Y., Bex, V., Midgley, P. M., Eds.; Cambridge University Press, 2013.

(3) Shindell, D. T.; Chin, M.; Dentener, F.; Doherty, R. M.; Faluvegi, G.; Fiore, A. M.; Hess, P.; Koch, D. M.; MacKenzie, I. A.; Sanderson, M. G.; et al. A multi-model assessment of pollution transport to the Arctic. *Atmopsheric Chem. Phys.* **2008**, *8*, 5353–5372.

(4) Bowerman, N. H. A.; Frame, D. J.; Huntingford, C.; Lowe, J. A.; Smith, S. M.; Allen, M. R. The role of short-lived climate pollutants in meeting temperature goals. *Nat. Clim. Chang.* **2013**, *3* (12), 1021–1024.

(5) Quinn, P. K.; Bates, T. S.; Baum, E.; Doubleday, N.; Fiore, A. M.; Flanner, M.; Fridlind, A.; Garrett, T. J.; Koch, D.; Menon, S.; et al. Short-lived pollutants in the Arctic: their climate impact and possible mitigation strategies. *Atmos. Chem. Phys.* **2008**, *8*, 1723–1735.

(6) Warren, S. G.; Wiscombe, W. J. A Model for the Spectral Albedo of Snow. II: Snow Containing Atmospheric Aerosols. *J. Atmos. Sci.* **1980**, *37*, 2734–2745.

(7) Flanner, M. G.; Zender, C. S.; Randerson, J. T.; Rasch, P. J. Present-day climate forcing and response from black carbon in snow. *J. Geophys. Res. Atmos.* **2007**, *112* (11), 1–17.

(8) Petzold, A.; Ogren, J. A.; Fiebig, M.; Laj, P.; Li, S. M.; Baltensperger, U.; Holzer-Popp, T.; Kinne, S.; Pappalardo, G.; Sugimoto, N.; et al. Recommendations for reporting black carbon measurements. *Atmos. Chem. Phys.* **2013**, *13* (16), 8365–8379.

(9) Popovicheva, O. B. Combustion-derived carbonaceous aerosols (soot) in the atmosphere: Water interaction and climate effects. In *Aerosol Science and Technology*; Agranovski, I., Ed.; Wiley - VCH Verlag GmbH & Co. KGaA, 2010; pp 127–157.

(10) Yun, Y.; Penner, J. E.; Popovicheva, O. The effects of hygroscopicity on ice nucleation of fossil fuel combustion aerosols in mixed-phase clouds. *Atmos. Chem. Phys.* **2013**, *13* (8), 4339–4348.

(11) Popovicheva, O.; Kistler, M.; Kireeva, E.; Persiantseva, N.; Timofeev, M.; Kopeikin, V.; Kasper-Giebl, A. Physicochemical characterization of smoke aerosol during large-scale wildfires: Extreme event of August 2010 in Moscow. *Atmos. Environ.* **2014**, *96* (August 2011), 405–414.

(12) Diapouli, E.; Popovicheva, O.; Kistler, M.; Vratolis, S.; Persiantseva, N.; Timofeev, M.; Kasper-Giebl, A.; Eleftheriadis, K. Physicochemical characterization of aged biomass burning aerosol after long-range transport to Greece from large scale wildfires in Russia and surrounding regions, Summer 2010. *Atmos. Environ.* **2014**, *96*, 393–404.

(13) Eleftheriadis, K.; Vratolis, S.; Nyeki, S. Aerosol black carbon in the European Arctic: Measurements at Zeppelin station, Ny-??lesund, Svalbard from 1998-2007. *Geophys. Res. Lett.* **2009**, *36* (2), 1–5.

(14) AMAP. *AMAP assessment 2015: Black carbon and ozone as Arctic climate forcers*; Arctic Monitoring and Assessment Programme (AMAP), Oslo, Norway, 2015.

(15) Wang, Q.; Chen, X. Nuclear accident like Fukushima unlikely in the rest of the world? *Environ. Sci. Technol.* **2011**, *45* (23), 9831–9832.

(16) Stohl, A.; Berg, T.; Burkhart, J. F.; Fjæraa, a. M.; Forster, C.; Herber, A.; Hov, Ø.; Lunder, C.; McMillan, W. W.; Oltmans, S.; et al. Arctic smoke – record high air pollution levels in the European Arctic due to agricultural fires in Eastern Europe. *Atmos. Chem. Phys. Discuss.* **2006**, *6* (5), 9655–9722.

(17) Stock, M.; Ritter, C.; Herber, A.; von Hoyningen-Huene, W.; Baibakov, K.; Gräser, J.; Orgis, T.; Treffeisen, R.; Zinoviev, N.; Makshtas, A.; et al. Springtime Arctic aerosol: Smoke versus haze, a case study for March 2008. *Atmos. Environ.* **2012**, *52* (March 2008), 48–55.

(18) Evangeliou, N.; Balkanski, Y.; Hao, W. M.; Petkov, A.; Silverstein, R. P.; Corley, R.; Nordgren, B. L.; Urbanski, S. P.; Eckhardt, S.; Stohl, A.; et al. Wildfires in northern Eurasia affect the budget of black carbon in the Arctic-a 12-year retrospective synopsis (2002-2013). *Atmos. Chem. Phys.* **2016**, *16* (12), 7587–7604.

(19) AMAP. *The Impact of Black Carbon on Arctic Climate (2011)*; Berntsen, T., Burkhart, J. F., Christensen, J., Flanner, M., Kupiainen, K., Lihavainen, H., Shepherd, M., Shevchenko, V., Skov, H., Vestreng, V., Eds.; Arctic Monitoring and Assessment Programme (AMAP), Oslo, Norway, 2011; Vol. 4.

(20) Cofala, J.; Amann, M.; Klimont, Z.; Kupiainen, K.; Höglund-Isaksson, L. Scenarios of global anthropogenic emissions of air pollutants and methane until 2030. *Atmos. Environ.* **2007**, *41* (38), 8486–8499.

(21) Stohl, A.; Klimont, Z.; Eckhardt, S.; Kupiainen, K.; Shevchenko, V. P.; Kopeikin, V. M.; Novigatsky, A. N. Black carbon in the Arctic: The underestimated role of gas flaring and residential combustion emissions. *Atmos. Chem. Phys.* **2013**, *13* (17), 8833–8855.

(22) Cheng, M. D. Geolocating Russian sources for Arctic black carbon. *Atmos. Environ.* **2014**, *92*, 398–410.

(23) Uttal, T.; Makshtas, A.; Laurila, T. The Tiksi International Hydrometeorological Observatory - An Arctic Members Partnership. *Bull. World Meteorol. Organ.* **2013**, *62* (1), 22–26.

(24) Winiger, P.; Andersson, A.; Eckhardt, S.; Stohl, A.; Semiletov, I. P.; Dudarev, O. V.; Charkin, A.; Shakhova, N.; Klimont, Z.; Heyes, C.; et al. Siberian Arctic black carbon sources constrained by model and observation. *Proc. Natl. Acad. Sci.* **2017**, 1–8.

(25) Huang, K.; Fu, J. S.; Prikhodko, V. Y.; Storey, J. M.; Romanov, A.; Hodson, E. L.; Cresko, J.; Morozova, I.; Ignatieva, Y.; Cabaniss, J. Russian anthropogenic black carbon: Emission reconstruction and Arctic black carbon simulation. *J. Geophys. Res. Atmos.* **2015**, *120* (21), 11306–11333.

(26) Huang, K.; Fu, J. S. Data Descriptor : A global gas fl aring black carbon emission rate dataset from 1994 to 2012. *Nature* **2016**, 1–11.

(27) Panchenko, M. V.; Kozlov, V. S.; Pol'kin, V. V.; Golobokova, L. P.; Pogodaeva, T. V.; Khodzher, T. V.; Lisitzin, A. P.; Shevchenko, V. P. Investigations of microphysical and chemical composition of aerosol in near-water layer of the atmosphere over the White Sea. *Proc. SPIE 6522, Thirteen. Jt. Int. Symp. Atmos. Ocean Opt. Atmos. Phys.* **2006**, *66221A*.

(28) Kopeikin, V. M.; Repina, I. A.; Grechko, E. I.; Ogorodnikov, B. I. Measurements of soot aerosol content in the near-water atmospheric layer in the southern and northern hemispheres. *Atmos. Ocean. Opt.* **2010**, *23* (6), 500–507.

(29) Sakerin, S. M.; Bobrikov, A. A.; Bukin, O. A.; Golobokova, L. P.; Pol'Kin, V. V.; Pol'Kin, V. V.; Shmirko, K. A.; Kabanov, D. M.; Khodzher, T. V.; Onischuk, N. A.; et al. On measurements of aerosol-gas composition of the atmosphere during two expeditions in 2013 along the Northern Sea Route. *Atmos. Chem. Phys.* **2015**, *15* (21), 12413–12443.

(30) Hansen, A. D. A.; Rosen, H. Horizontal inhomogeneities in the particulate carbon component of the Arctic haze. *Atmos. Environ.* **1985**, *19* (12), 2175–2180.

(31) Drinovec, L.; Močnik, G.; Zotter, P.; Prévôt, A. S. H.; Ruckstuhl, C.; Coz, E.; Rupakheti, M.; Sciare, J.; Müller, T.; Wiedensohler, A.; et al. The "dual-spot" Aethalometer: An improved measurement of aerosol black carbon with real-time loading compensation. *Atmos. Meas. Tech.* **2015**, *8* (5), 1965–1979.

(32) Zanatta, M.; Gysel, M.; Bukowiecki, N.; M??ller, T.; Weingartner, E.; Areskoug, H.; Fiebig, M.; Yttri, K. E.; Mihalopoulos, N.; Kouvarakis, G.; et al. A European aerosol phenomenology-5: Climatology of black carbon optical properties at 9 regional background sites across Europe. *Atmos. Environ.* **2016**, *145*, 346–364.

(33) Stohl, A.; Hittenberger, M.; Wotawa, G. Validation of the lagrangian particle dispersion model FLEXPART against large-scale tracer experiment data. *Atmos. Environ.* **1998**, *32* (24), 4245–4264.

(34) Stohl, a.; Forster, C.; Frank, A.; Seibert, P.; Wotawa, G. Technical note: The Lagrangian particle dispersion model FLEXPART version 6.2. *Atmos. Chem. Phys. Discuss.* **2005**, *5* (4), 4739–4799.

(35) Stohl, A.; Forster, C.; Eckhardt, S.; Spichtinger, N.; Huntrieser, H.; Heland, J.; Schlager, H.; Wilhelm, S.; Arnold, F.; Cooper, O. A backward modeling study of intercontinental pollution transport using aircraft measurements. *J. Geophys. Res. Atmos.* **2003**, *108* (D12), 4370.

(36) Stohl, A.; Aamaas, B.; Amann, M.; Baker, L. H.; Bellouin, N.; Berntsen, T. K.; Boucher, O.; Cherian, R.; Collins, W.; Daskalakis, N.; et al. Evaluating the climate and

509 air quality impacts of short-lived pollutants. *Atmos. Chem. Phys.* **2015**, *15* (18), 10529–
510 10566.

511 (37) van der Werf, G. R.; Randerson, J. T.; Giglio, L.; Collatz, G. J.; Kasibhatla, P. S.;
512 Arellano, A. F., J. Interannual variability in global biomass burning emissions from
513 1997 to 2004. *Atmos. Chem. Phys.* **2006**, *6* (11), 3423–3441.

514 (38) Slinn, W. G. N. Predictions for particle deposition to vegetative canopies. *Atmos.*
515 *Environ.* **1982**, *16*, 1785–1794.

516 (39) Shiraiwa, M.; Kondo, Y.; Moteki, N.; Takegawa, N.; Sahu, L. K.; Takami, A.;
517 Hatakeyama, S.; Yonemura, S.; Blake, D. R. Radiative impact of mixing state of black
518 carbon aerosol in Asian outflow. *J. Geophys. Res. Atmos.* **2008**, *113* (24), 1–13.

519 (40) Grythe, H.; Kristiansen, N. I.; Groot Zwaaftink, C. D.; Eckhardt, S.; Ström, J.; Tunved,
520 P.; Krejci, R.; Stohl, A. A new aerosol wet removal scheme for the Lagrangian particle
521 model FLEXPART. *Geosci. Model Dev. Discuss.* **2016**, No. October, 1–34.

522 (41) Eckhardt, S.; Quennehen, B.; Olivié, D. J. L.; Berntsen, T. K.; Cherian, R.;
523 Christensen, J. H.; Collins, W.; Crepinsek, S.; Daskalakis, N.; Flanner, M.; et al.
524 Current model capabilities for simulating black carbon and sulfate concentrations in the
525 Arctic atmosphere: A multi-model evaluation using a comprehensive measurement
526 data set. *Atmos. Chem. Phys.* **2015**, *15* (16), 9413–9433.

527 (42) Stone, R. S.; Sharma, S.; Herber, A.; Eleftheriadis, K.; Nelson, D. W. A
528 characterization of Arctic aerosols on the basis of aerosol optical depth and black
529 carbon measurements. *Elem. Sci. Anthr.* **2014**, *2*, 1–22.

530

## FIGURE CAPTIONS FOR MANUSCRIPT

**Figure 1. (a)** Time series of equivalent black carbon (EBC) mass concentrations during the expedition cruise. Numbers and letters in red brackets show geographical names during the cruise according to Figure S 1. **(b)** Age spectra of modeled BC (colors) from all possible sources showing the contribution of emissions each day back in time to the surface concentration of BC. Hourly means of measured BC concentrations are shown as a black line. **(c)** Contribution from different emission source types to the BC surface concentrations. The emission sources of biomass burning (BB), waste burning (WST), industrial combustion and processing (IND), surface transportation (TRA), power plants, energy conversion, and extraction (ENE), and residential and commercial (DOM) have been adopted from GFEDv3.1 and ECLIPSE inventories [36,37]. Notice the different scale used in all three panels from 24 to 25 October, when measured and modeled concentrations were much higher than for the rest of the cruise. Flaring emissions are included in the energy sector (ENE).

**Figure 2. (a)** Footprint emission sensitivity and **(b)** contribution from anthropogenic sources to surface BC concentrations on 12 October 2015 at 05:00. **(c)** Footprint emission sensitivity and **(d)** contribution from anthropogenic sources to surface BC concentrations on 13 October 2015 at 11:44. Values written in black report the simulated concentration of BC at the receptor (ship) for the same time period from all anthropogenic sources, while colored ones denote the continental contribution from anthropogenic sources. Magenta shows contribution from South America, orange from Europe, yellow from Australia, green from North America, cyan from Africa and blue from Asia.

**Figure 3.** Daily average footprint emission sensitivities when the vessel **(a)** arrived (14 October 2015) and **(b)** departed (18 October 2015) from the "Ice Base Cape Baranova" station.

**Figure 4. (a)** Footprint emission sensitivity when the ship had passed the Dvina River and before arrival to the port of Arkhangelsk (25 October 2015 00:00). **(b)** Contribution from anthropogenic sources and **(c)** biomass burning to the simulated surface concentration of BC at the same date and time. Black values show the concentration of BC at the receptor (ship) for the time period from all anthropogenic and biomass burning sources. Colored values denote continental contribution from anthropogenic sources; magenta show contribution from

562 South America, orange from Europe, yellow from Australia, green from North America, cyan
563 from Africa and blue from Asia.

564 **Figure 5.** Distribution of normalized bias, i.e., (model-observed)/observed, for the measured
565 EBC and the BC concentrations predicted by FLEXPART. The biases were calculated for the
566 daily average concentrations and for the ship location at midnight of each day (00:00).

567

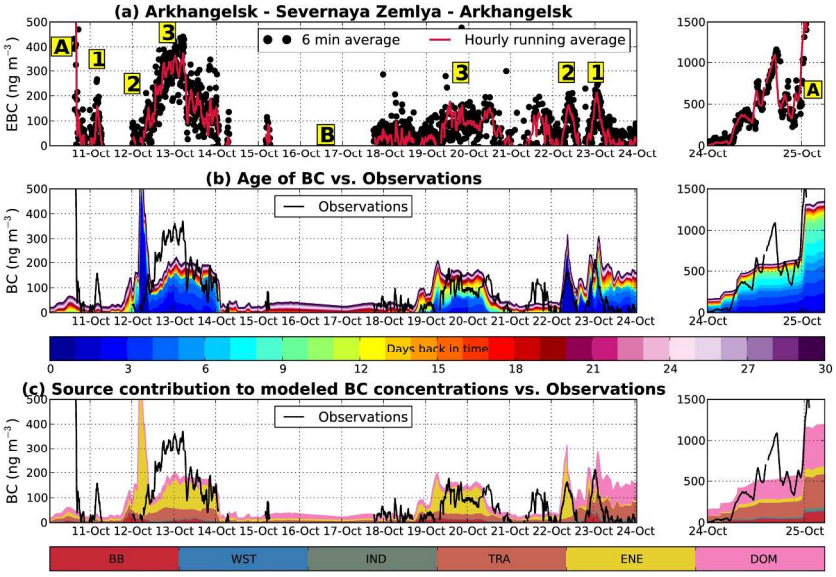


(a) Time series of equivalent black carbon (EBC) mass concentrations during the expedition cruise. Numbers and letters in red brackets show geographical names during the cruise according to Figure S 1. (b) Age spectra of modeled BC (colors) from all possible sources showing the contribution of emissions each day back in time to the surface concentration of BC. Hourly means of measured BC concentrations are shown as a black line. (c) Contribution from different emission source types to the BC surface concentrations. The emission sources of biomass burning (BB), waste burning (WST), industrial combustion and processing (IND), surface transportation (TRA), power plants, energy conversion, and extraction (ENE), and residential and commercial (DOM) have been adopted from GFEDv3.1 and ECLIPSE inventories 36,37. Notice the different scale used in all three panels from 24 to 25 October, when measured and modeled concentrations were much higher than for the rest of the cruise. Flaring emissions are included in the energy sector (ENE).

Figure 1

261x182mm (300 x 300 DPI)

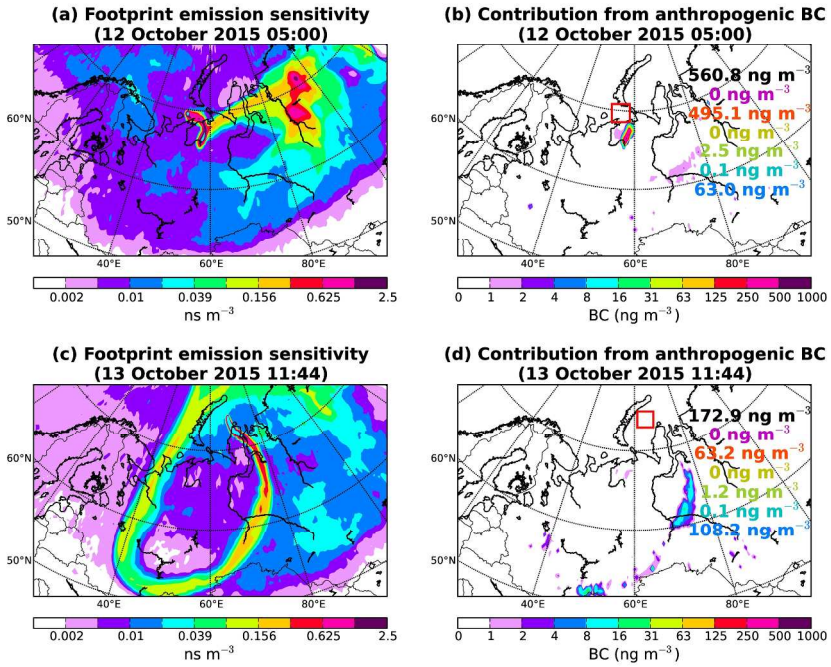


(a) Footprint emission sensitivity and (b) contribution from anthropogenic sources to surface BC concentrations on 12 October 2015 at 05:00. (c) Footprint emission sensitivity and (d) contribution from anthropogenic sources to surface BC concentrations on 13 October 2015 at 11:44. Values written in black report the simulated concentration of BC at the receptor (ship) for the same time period from all anthropogenic sources, while colored ones denote the continental contribution from anthropogenic sources. Magenta shows contribution from South America, orange from Europe, yellow from Australia, green from North America, cyan from Africa and blue from Asia.

Figure 2
275x214mm (300 x 300 DPI)

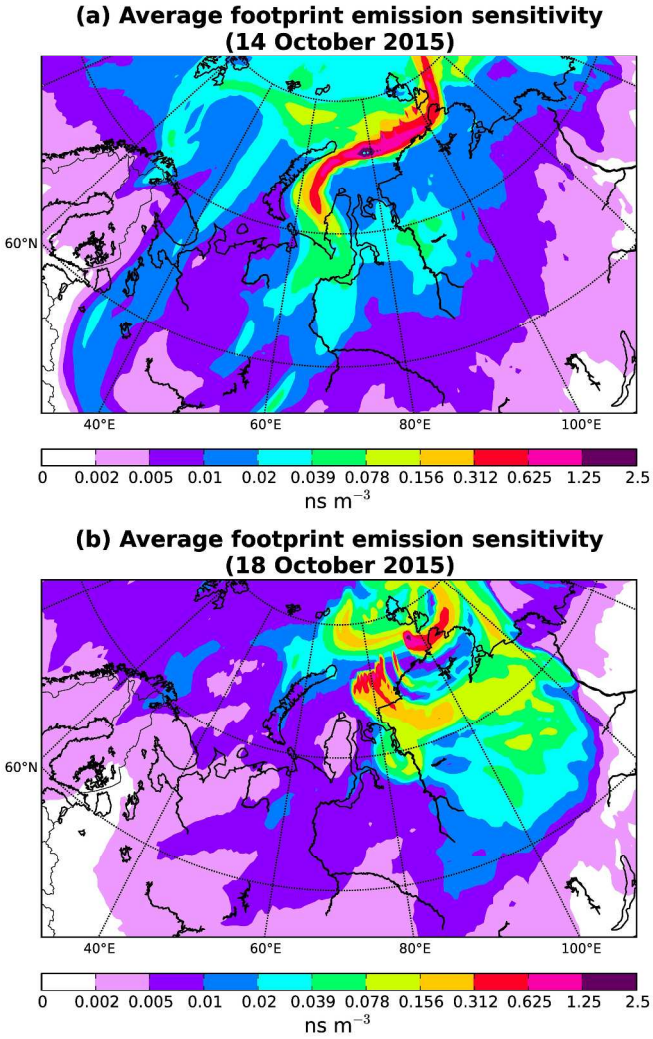


Daily average footprint emission sensitivities when the vessel (a) arrived (14 October 2015) and (b) departed (18 October 2015) from the "Ice Base Cape Baranova" station.
Figure 3
320x500mm (300 x 300 DPI)

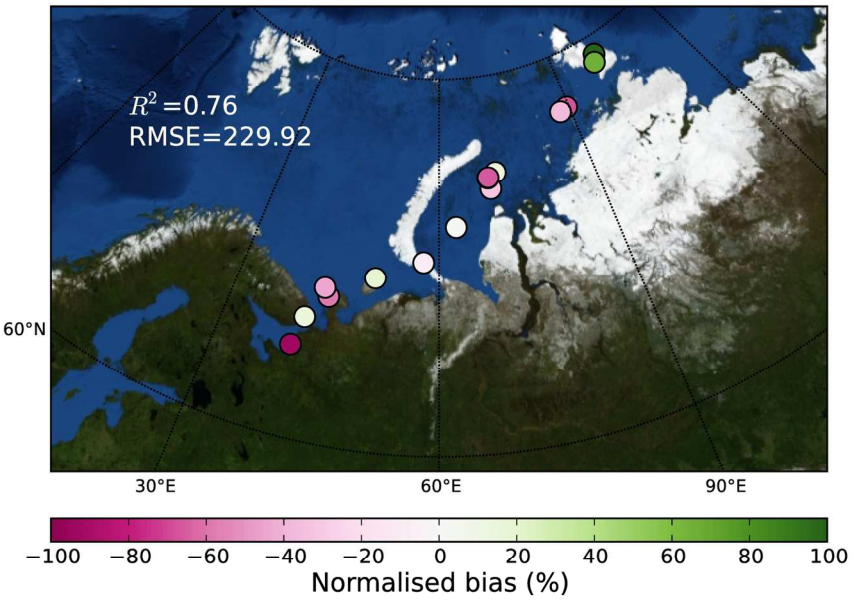


Distribution of normalized bias, i.e., (model-observed)/observed, for the measured EBC and the BC concentrations predicted by FLEXPART. The biases were calculated for the daily average concentrations and for the ship location at midnight of each day (00:00).
Figure 5
155x117mm (300 x 300 DPI)

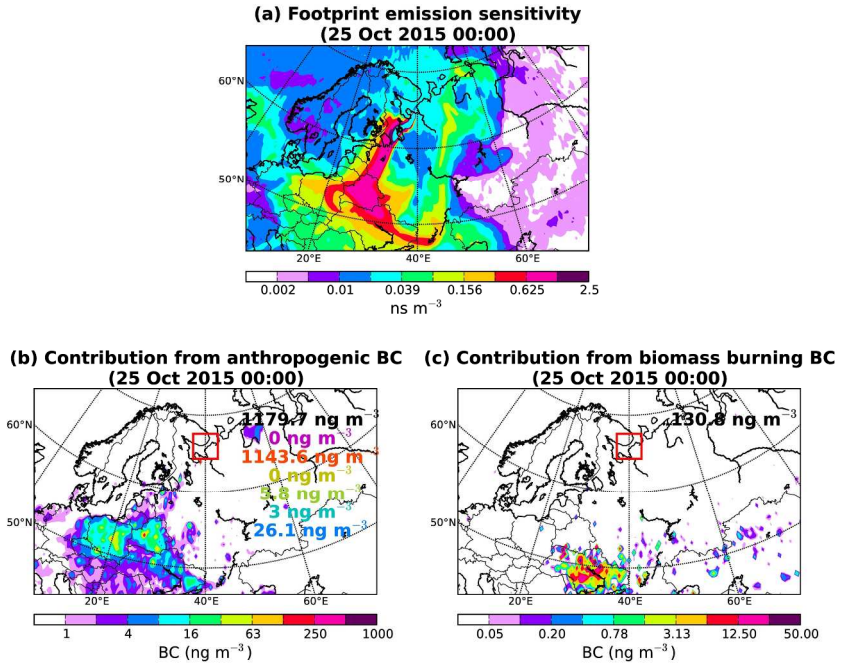


(a) Footprint emission sensitivity when the ship had passed the Dvina River and before arrival to the port of Arkhangelsk (25 October 2015 00:00). (b) Contribution from anthropogenic sources and (c) biomass burning to the simulated surface concentration of BC at the same date and time. Black values show the concentration of BC at the receptor (ship) for the time period from all anthropogenic and biomass burning sources. Colored values denote continental contribution from anthropogenic sources; magenta show contribution from South America, orange from Europe, yellow from Australia, green from North America, cyan from Africa and blue from Asia.

Figure 4
248x180mm (300 x 300 DPI)

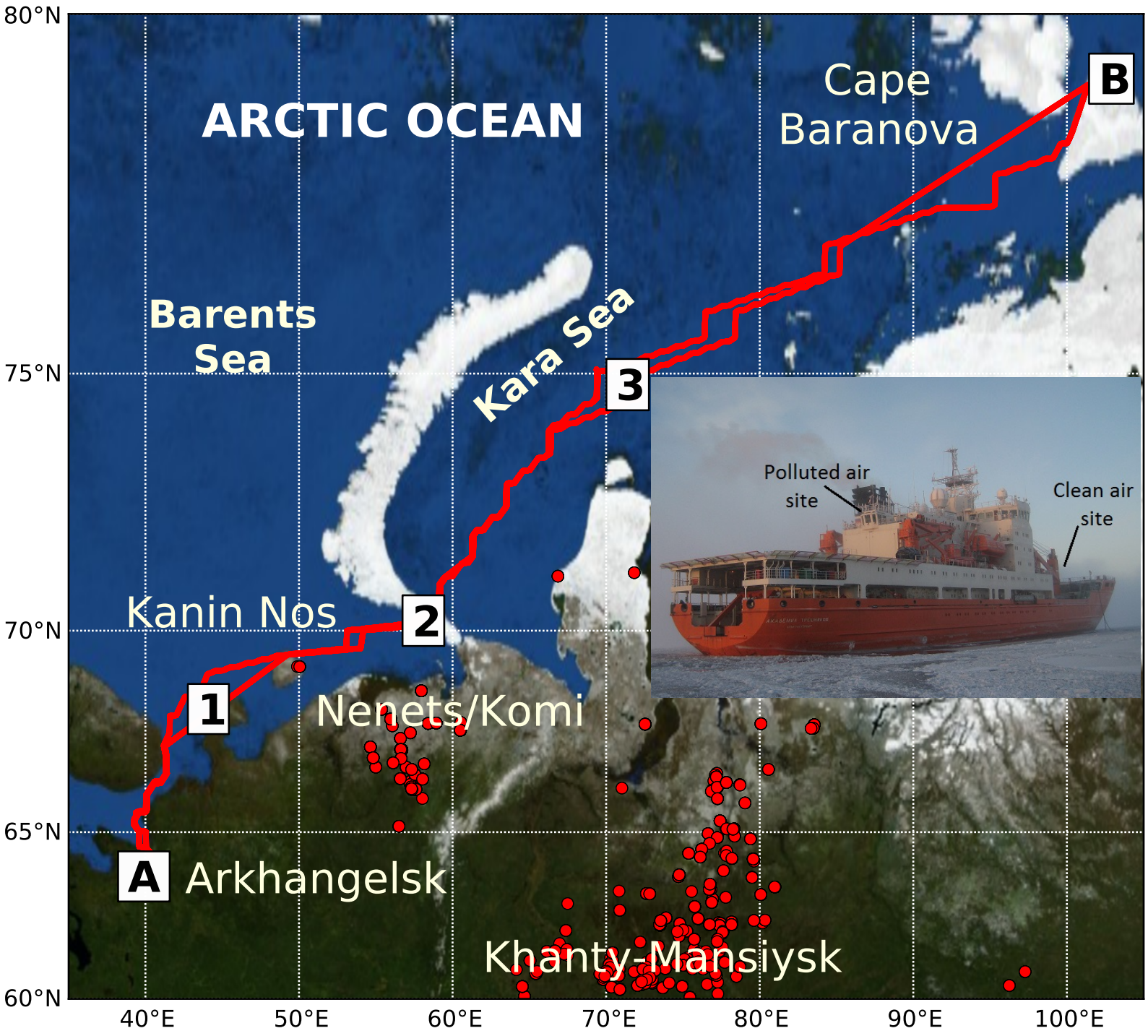
80°N
75°N
70°N
65°N
60°N
40°E
50°E
60°E
70°E
80°E
90°E
100°E
ARCTIC OCEAN
Barents Sea
Kara Sea
Cape Baranova
B
3
2
1
A
Kanin Nos
Nenets/Komi
Arkhangelsk
Khanty-Mansiysk
Polluted air site
Clean air site